Measuring Dark Energy Clustering with CMB-Galaxy Correlations

Wayne Hu[1], Ryan Scranton[2]
[1]*Kavli Institute for Cosmological Physics, Department of Astronomy & Astrophysics, Enrico Fermi Institute, University of Chicago, Chicago IL 60637*
[2]*University of Pittsburgh, Department of Physics and Astronomy, Pittsburgh, PA 15260*

The integrated Sachs-Wolfe (ISW) effect in the cosmic microwave background (CMB) as measured through its correlation with galaxies provides a unique opportunity to study the dynamics of the dark energy through its large scale clustering properties. Ultimately, a deep all-sky galaxy survey out to $z \sim 2$ can make a $\sim 10\sigma$ or $\sim 10\%$ measurement of the correlation and limit $\sim 3\%$ changes in the gravitational potential or total density fluctuation due to dark energy clustering on the Gpc scale. A canonical single scalar field or quintessence model predicts that these clustering effects will appear on the horizon scale with a strength that reflects the evolution of the dark energy density. In terms of a constant equation of state, this would allow tests of the quintessence prediction for models where $|1 + w| \gtrsim 0.05$.

I. INTRODUCTION

The two generic signatures of a dynamical form of the dark energy are an energy density that evolves as a function of time and one that varies as a function of space. Clustering in the dark energy is in fact an unavoidable consequence of time evolution on superhorizon scales. Prospects for measuring the density evolution or equation of state of the dark energy are well known. Detecting its spatial clustering is considerably harder but of at least equal fundamental importance. In particular, the clustering tests the quintessence hypothesis, dark energy as a single scalar field with a canonical kinetic term [1, 2].

Perhaps the best hope of studying the clustering of the dark energy lies in its effect on the cosmic microwave background (CMB). In general, the effect of having a "smooth" component that alters the expansion rate without clustering with the dark matter is to make gravitational potentials decay in the linear regime. As a CMB photon transits a decaying potential well, it picks up a net blueshift. When integrated across the potential hills and wells along the line of sight, this effect leaves a temperature anisotropy across the line of sight called the integrated Sachs Wolfe (ISW) effect [3, 4]. On scales where the dark energy is clustered, this effect is reduced in a potentially measurable way. It is a curious coincidence that the observed large angle temperature anisotropy is also suppressed compared with a cosmological constant model (e.g. [5] and [6, 21] for a possible ISW connection).

Since the decay of the gravitational potential is a direct consequence of the dark energy, the ISW effect is more sensitive to changes in the clustering of the dark energy than other clustering statistics. Unfortunately this sensitivity is hidden in the CMB by the anisotropy from recombination. The ISW contributions can be isolated by cross correlating the temperature field with other tracers of the gravitational potential, in particular galaxies [7] and gravitational lensing statistics [8, 9, 10].

Recently the ISW effect has been detected by cross correlating temperature maps from WMAP with radio galaxies, optical galaxies, infra-red galaxies and X-ray sources [11, 12, 13, 14]. The current measurements are not sufficient for much beyond a simple detection of the effect, but do indicate that the technical issues involved are well within in the capabilities of current and future surveys.

In this paper we study the prospects for constraining the smoothness of the dark energy with future galaxy surveys. This study extends that of Afshordi [15] who mainly considered prospects for constraining the equation of state of the dark energy under the small scale Limber approximation. ISW constraints on a smooth equation of state are not competitive with other probes of dark energy evolution due to the unavoidable cosmic variance of the CMB temperature field, whereas they may provide the best means of studying the clustering of the dark energy.

The outline of the paper is as follows. In §II, we review the predictions and parameterization of the large scale clustering of the dark energy. In §III, we calculate the ISW-galaxy correlation under the general all-sky framework applicable to correlated galaxy distributions and fine redshift resolution. In §IV we study the potential of galaxy surveys to constrain the clustering of the dark energy.

II. DARK ENERGY CLUSTERING

With adiabatic initial conditions and in the absence of non-gravitational forces, all energy density components, including the dark energy, are clustered. In this limit, the gravitational potential or Newtonian curvature Φ evolves

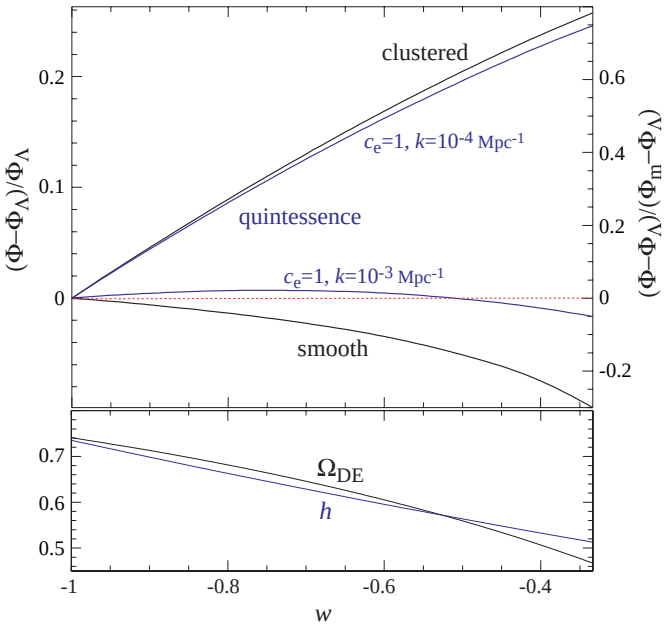

FIG. 1: Fractional difference in the gravitational potential today between smooth and clustered dark energy models as a function of w (upper panel) where $\Omega_{\rm DE}$ and h are adjusted to keep the distance to recombination and the expansion rate at high-z fixed. Also shown are the predictions for quintessence dark energy (canonical kinetic term with sound speed $c_e = 1$) near the horizon scale $k = 10^{-4}$ Mpc^{-1} and near the broad peak of the ISW effect at low multipoles $k = 10^{-3}$ Mpc^{-1}.

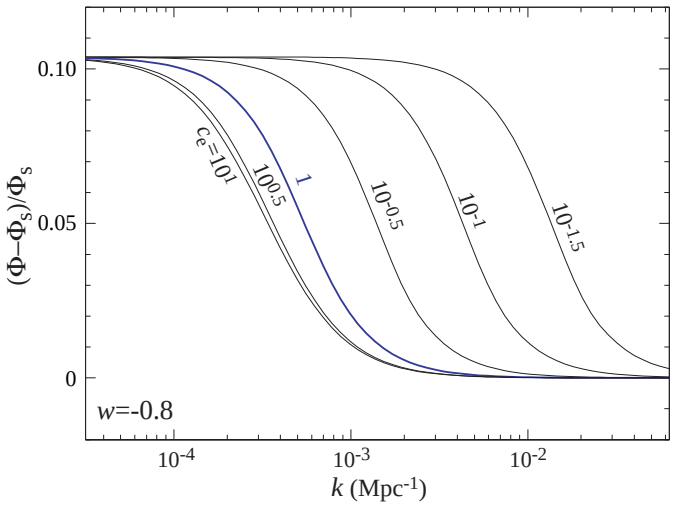

FIG. 2: Fractional change in the gravitational potential in the transition regime between smooth (Φ_s) and clustered dark energy for several choices of the sound speed and a $w = -0.8$ model. The quintessence prediction corresponds to $c_e = 1$.

in a flat universe according to the relation [16, 17]

$$\Phi = \left(1 - \frac{H(a)}{a}\int_0^a \frac{da'}{H(a')}\right)\zeta_i\,, \qquad (1)$$

where ζ_i is the initial comoving curvature and H is the Hubble parameter. Note that during epochs when the expansion is dominated by a species with a constant equation of state parameter $w_T = p_T/\rho_T$, $H(a) \propto a^{-3(1+w_T)/2}$ and the gravitational potential is constant

$$\Phi = \frac{3(1+w_T)}{5+3w_T}\zeta_i\,. \qquad (2)$$

With only gravitational forces, the ISW effect vanishes in a flat, constant w_T universe except for the special case of $w_T = -1$ where the constant is zero.

To accelerate the expansion, dark energy requires relativistic stresses where the pressure is comparable to the energy density in magnitude. Stress gradients can prevent the clustering of the dark energy on small scales. Given dark energy that is smooth compared with the dark matter, the gravitational potential evolves in a flat universe as

$$\frac{d^2\Phi}{d\ln a^2} + \left[\frac{5}{2} - \frac{3}{2}w(a)\Omega_{\rm DE}(a)\right]\frac{d\Phi}{d\ln a} + \frac{3}{2}[1-w(a)]\Omega_{\rm DE}(a)\Phi = 0\,. \qquad (3)$$

Here $w(a) = p_{\rm DE}/\rho_{\rm DE}$ is the equation of state for the dark energy and $\Omega_{\rm DE}(a) = \rho_{\rm DE}(a)/\rho_{\rm crit}(a)$. Where no argument is given $a = 1$ is assumed and the Hubble constant $H_0 = H(a = 1) = 100h$ km s^{-1} Mpc^{-1}. The initial conditions for scales well above the horizon at matter-radiation equality are provided by Eq. (1) with a starting epoch in the matter-dominated limit. For smaller scales, the initial conditions are modified by the usual transfer function to account for radiation stresses.

In Fig. 1 (upper panel), we show the fractional difference in the gravitational potential today for the smooth and clustered regime relative to a cosmological constant $w = -1$ model. In this model Φ has decayed from $\Phi_m = 3\zeta_i/5$ in the matter dominated $w_T = 0$ regime to $\Phi_\Lambda = 0.75\Phi_m$ by the present.

On the right axis, we normalize the curves relative to the net change in the gravitational potential $\Phi_m - \Phi_\Lambda = 0.25\Phi_m$ in the $w = -1$ model. Since the ISW effect is sensitive to the change in the gravitational potential, this factor of 3 enhancement of the difference reflects the observational effect. This enhancement is the reason why the ISW effect is more sensitive to dark energy clustering than other measures of clustering.

Note that here and throughout when considering models of different w, $\Omega_{\rm DE}$ and h are adjusted to keep the well-constrained distance to recombination and high redshift expansion rate fixed (Fig 1, lower panel). This adjustment guarantees that the CMB predictions for the various dark energy models will be indistinguishable aside from the ISW effect of interest (see also Fig. 3).

The transition between the smooth and clustered regimes depends on the physical model for the dark energy. It is usefully parameterized by the effective sound

speed of the dark energy c_e, defined through

$$c_e^2 = \frac{\delta p_{\rm DE}}{\delta \rho_{\rm DE}} \tag{4}$$

in a "rest frame" coordinate system where the momentum density of the dark energy vanishes [2]. In terms of the gravitational potential phenomenology, the minimum of the sound horizon and (particle) horizon separates the smooth and clustered regime. Above the horizon, there is no unique definition of smoothness for a dark energy component whose density varies with time given the freedom to choose the time slicing in general relativity [1].

In a scalar field dark energy model, the sound speed so defined is exactly given in linear theory by the form of the kinetic energy as a function of the field [18, 19]. For a canonical kinetic term, the sound speed $c_e = 1$. As a dark energy candidate, a canonical scalar field is dubbed quintessence and one with an alternative kinetic term k-essence [20]. For quintessence, the transition between the smooth and clustered regimes thus occurs near the horizon scale. In Fig. 1, we also show the gravitational potential amplitude for a scalar field model at $k = 10^{-3}$ Mpc^{-1} and $k = 10^{-4}$ Mpc^{-1}. Note that the horizon scale

$$\eta_0 = \int_0^1 \frac{dt}{a} \approx 14{\rm Gpc}\,, \tag{5}$$

and so the horizon wavenumber $k_H \equiv \eta_0^{-1} \approx 7\times10^{-5}$ Mpc^{-1}. In the $w = -1$ model contributions to the ISW effect at the scale of the quadrupole are broadly distributed around $k = 10^{-3}$ Mpc^{-1} due to projection effects (see e.g. [21]). Thus a fair fraction of the contributions to the ISW effect will come from the transition regime if $w \neq -1$ (e.g. [2, 10, 22]).

In Fig. 2, we show the effect of dark energy clustering as a function of scale for $c_e = 10^{-1.5}, 10^{-1} \ldots 10^{1}$ for $w = -0.8$ the smooth limit Φ_s of Eq. (3). We employ these numerical results for the potential spectrum at the present in the following sections. For the time evolution employed in the next section, we use the interpolation between solutions of the clustered and smooth regimes in Eq. (1) and (3) given in [10], valid for $c_e \leq 1$.

Note that the clustering effects saturate close to $c_e = 1$. For this reason, we will take models with $c_e \leq 1$. For illustrative purposes we will also typically employ the $w = -0.8$ model but discuss the conversion of constraints to general dark energy models in §IV.

III. ISW CROSS-CORRELATION

The effects of dark energy clustering can be seen on the two-point correlation between observed fields that depend on the gravitational potential such as the CMB temperature and the galaxy number density. Let us assume that a field $x(\hat{\mathbf{n}})$ as a function of the angular position $\hat{\mathbf{n}}$ on the sky is a weighted projection of the potential field $\Phi(\mathbf{x}; z)$

$$x(\hat{\mathbf{n}}) = \int dz W^x(D\hat{\mathbf{n}}; z)\Phi(D\hat{\mathbf{n}}; z)\,, \tag{6}$$

where the weight W^x can include differential operators acting on the field. Here $D = \int_0^z dz/H(a)$ is the comoving distance to redshift z. Then the angular cross correlation between two observed fields x and x' is given by

$$\langle x(\hat{\mathbf{n}})x'(\hat{\mathbf{n}}')\rangle = \sum_\ell P_\ell(\hat{\mathbf{n}}\cdot\hat{\mathbf{n}}')\frac{2\ell+1}{4\pi}C_\ell^{xx'}\,, \tag{7}$$

where P_ℓ is the Legendre polynomial and $C_\ell^{xx'}$ is the cross power spectrum. The angular power spectrum itself is given by

$$C_\ell^{xx'} = 4\pi\int\frac{d^3k}{(2\pi)^3}I_\ell^x(k)I_\ell^{x'}(k)P^{\Phi\Phi}(k;0)\,, \tag{8}$$

where $P^{\Phi\Phi}(k; z)$ is the 3D power spectrum of the potential field

$$\langle\Phi(\mathbf{k};0)\Phi(\mathbf{k}';0)\rangle = (2\pi)^3\delta(\mathbf{k}-\mathbf{k}')P^{\Phi\Phi}(k;0) \tag{9}$$

and the weights

$$I_\ell^x(k) = \int dz\frac{\Phi(k;z)}{\Phi(k;0)}W^x(k;z)j_\ell(kD)\,. \tag{10}$$

For the ISW effect

$$W^I(k;z) = 2\frac{\partial\ln\Phi}{\partial z}\,. \tag{11}$$

Note that in spite of the fact that in reasonable dark energy models the gravitational potential changes most rapidly around the current epoch, the local contributions to the angular power spectrum are strongly suppressed by the j_ℓ projection factors. The contributions from finite k locally appear in the monopole moment of the temperature field which makes a small and inseparable contribution to the background temperature.

In Fig. 3 we show CMB temperature power spectra for the $w = -0.8$ ($\Omega_{\rm DE} = 0.68$) model with the ISW contribution separated out for $c_e = 1$ and $c_e = 0.1$. In addition to the dark energy parameters, we will assume a physical non-relativistic matter density of $\Omega_m h^2 = 0.14$, a physical baryon density of $\Omega_b h^2 = 0.024$, a reionization optical depth of $\tau = 0.17$, an initial scale invariant comoving curvature spectrum with amplitude $\delta_\zeta = 5.07\times10^{-5}$ (WMAP $A = 0.87$ [24]) and slope $n = 1$.

Although the ISW contributions for the two models in Fig. 3 differ by up to a factor of 2 as is consistent with Fig. 1, the difference in the total temperature field is considerably less due to contributions from other effects. Given the cosmic variance of the temperature field also shown, the subtle difference is difficult to detect from the CMB alone.

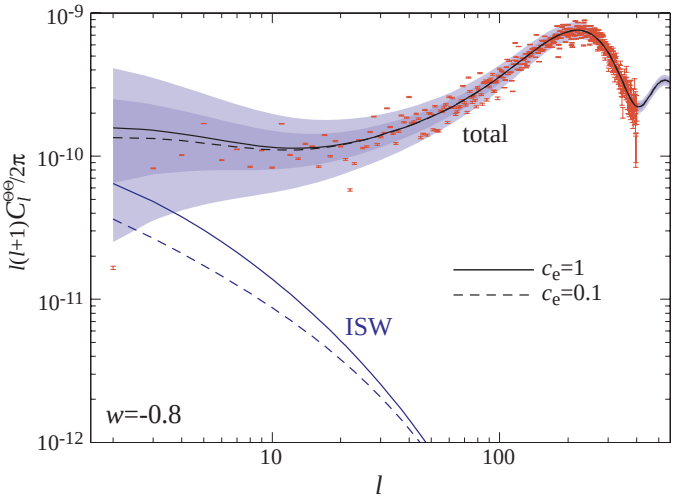

FIG. 3: CMB temperature power spectrum for the $w = -0.8$ model compared with the WMAP 1 year data with noise errors and the 68% and 95% cosmic variance confidence bands plotted for $c_e = 1$. The $c_e = 0.1$ model is difficult to distinguish from the $c_e = 1$ model even with perfect data despite the fact that the ISW effect changes by up to a factor of 2.

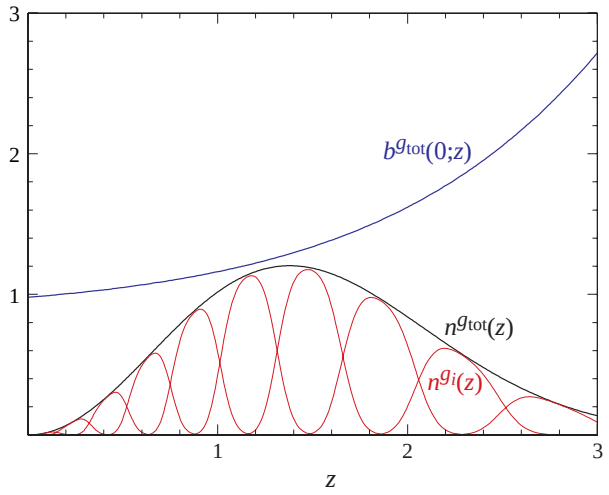

FIG. 4: Bias and redshift distribution of the galaxies. The total number density $n^{g_{\rm tot}}$ (here multiplied by $2/n_A^{g_{\rm tot}}$, with $n_A = 70$ gal arcmin^{-2} for clarity) defines the linear bias $b^{n_{\rm tot}}(0;z)$ under the halo model [23]. This total number density is divided into photometric redshift bins of $5\sigma(z)$ with photometric redshift errors of $\sigma(z) = 0.03(1+z)$.

The intrinsic sensitivity of the ISW effect to dark energy clustering can be extracted from cross correlations with the galaxy number density fluctuations. For the galaxy clustering, there is a number density fluctuation field for each population of galaxies. We denote the ith population as having a number density fluctuation g_i. The weights are given by

$$W^{g_i}(k;z) = \frac{n^{g_i}(z)}{n_A^i}\frac{2}{3}\left(\frac{k}{H_0}\right)^2\frac{a}{\Omega_m}b^{g_i}(k;z)\,, \qquad (12)$$

where the $n^{g_i}(z)$ is the redshift distribution of the population with an angular number density of $\int dz\, n^{g_i}(z) = n_A^i$ and $b^{g_i}(k;z)$ is the galaxy bias of the population. For the galaxy bias we take the parameterized halo model described in [23]. As long as galaxy number fluctuations trace the total density fluctuation or gravitational potential in the linear regime, the details of this model do not affect the end results. This is because in the linear regime, the galaxy auto correlation $C_\ell^{g_i g_j}$ determines the bias parameters for the ISW-galaxy cross correlation. Marginalization of halo parameters mainly eliminates the small amount of information coming from the non-linear regime.

For illustrative purposes, let us take populations to be selected from an overall redshift distribution of the form

$$n^{g_{\rm tot}}(z) \propto z^2 e^{-(z/z_n)^2}\,, \qquad (13)$$

with z_n adjusted to give a median redshift of $z = 1.5$ and a total galaxy number density of $n_A^{\rm tot} = 70$ gal/arcmin^2. Under the halo model of [23] this number density determines the linear bias shown in Fig. 4. These specifications are close to what can be achieved from an LSST type survey [25]. This parent distribution can be subdivided into multiple populations

$$n^{g_{\rm tot}}(z) = \sum_i n^{g_i}(z) \qquad (14)$$

through photometric redshifts. To approximate the redshift binning, let us suppose that photometric redshift estimates are distributed as a Gaussian with an rms fluctuation of $\sigma(z)$. A top hat cut in photometric redshift then becomes smooth overlapping distributions in actual redshift

$$n^{g_i}(z) = \frac{1}{2}n^{g_{\rm tot}}(z)\left[{\rm erfc}\left(\frac{z_{i-1}-z}{\sqrt{2}\sigma(z)}\right) - {\rm erfc}\left(\frac{z_i - z}{\sqrt{2}\sigma(z)}\right)\right], \qquad (15)$$

where erfc is the complementary error function. We take as a fiducial model $\sigma(z) = 0.03(1+z)$ and choose the binning to span $5\sigma(z)$ for a total of 5 bins out to $z = 1$ and 10 bins out to $z = 3$ (see Fig. 4).

In Fig. 5, we show the cross power spectra of these binned galaxy fields with the ISW effect in the upper panel for $w = -0.8$ and $c_e = 1$ and in the lower panel the ratio of spectra for $c_e = 0.1$ and this model. Note that due to projection effects, the correlation in the higher redshift bins peak at higher ℓ or smaller angular scales where the cosmic variance is smaller.

The amplitude of the effect on the cross correlation as parameterized by c_e depends strongly on the background equation of state. In Fig. 6 we show the cross correlation of the $z = 0.75 - 1$ galaxy bin for $w = -1$, -0.8, -0.6, -0.4. Note that the variations between the models at $c_e = 1$ are relatively small (upper panel) whereas the

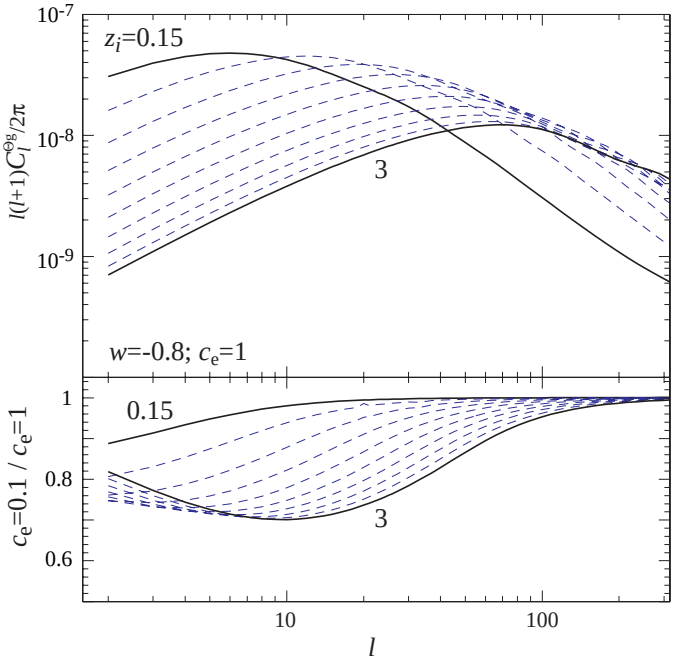

FIG. 5: Galaxy-CMB cross correlation through the ISW effect for the $w = -0.8$ model. Upper panel: $c_e = 1$ cross power spectra for 10 different galaxy redshift populations of Fig. 4. Lower panel: ratio of the $c_e = 0.1$ and $c_e = 1$ power spectra. Note that the intrinsic 10% change in the gravitational potential has been amplified by up to a factor of 3 through the sensitivity of the ISW effect to changes in the gravitational potential.

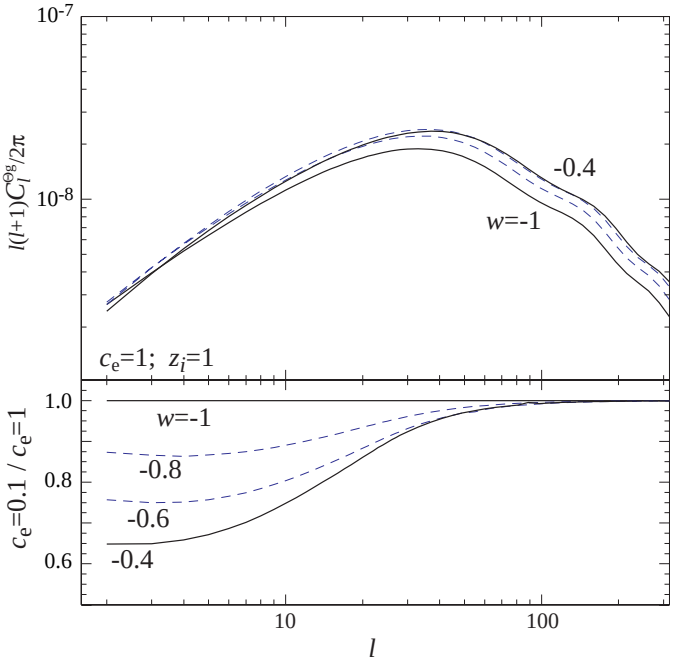

FIG. 6: Galaxy-CMB cross correlation as a function of w with the high-z universe fixed as in Fig. 1. The cross correlation itself is fairly insensitive to the equation of state for fixed sound speed ($c_e = 1$ upper panel) but becomes increasingly more sensitive to the sound speed as w increases.

difference between $c_e = 1$ and $c_e = 0.1$ increases as w increases. The consequence is that the cross correlation is a relatively insensitive probe of the dark energy equation of state given the fixed angular diameter distance to recombination and is mainly useful as a probe of dark energy clustering.

IV. CLUSTERING FORECASTS

Interpreting forecasts for the detectability of dark energy clustering requires special care for several reasons. Aside from the special case of a cosmological constant, no physical model can keep the dark energy smooth near or above the horizon scale. It is therefore not physically meaningful to compare a given dark energy model with and without dark energy perturbations. Although the sound speed parameterizes the physical scale of the transition to smoothness below the horizon, the amplitude of the transition depends strongly on the dark energy equation of state w for adiabatic initial conditions or tracking models which lose their dependence on initial fluctuations. Since changing the sound speed can shift the effect outside of an observed range, differences in models around a point in the parameter space do not reveal global constraints.

For these reasons, constraints involving the sound speed should be translated into statements as to how smooth the dark energy is out to a given physical scale. Such statements will also retain greater validity outside of the adiabatic and constant sound speed class of models.

With this in mind let us begin with the usual Fisher approach to parameter estimation forecasts. Consider the a survey which makes noisy measurements of a set of fields x_i with a noise power spectra of $N_l^{x_i x_j}$. Then the total, signal plus noise, power spectra are given by

$$\tilde{C}_l^{x_i x_j} = C_l^{x_i x_j} + N_l^{x_i x_j} \,. \tag{16}$$

Given a parameterization of the signal power spectrum with a set of parameters p_α, the information in the survey on these parameters is quantified by the Fisher matrix

$$F_{\alpha\beta} = f_{\rm sky} \sum_l \frac{(2l+1)\Delta l}{2} \, {\rm Tr}[\mathbf{D}_{l\alpha} \tilde{\mathbf{C}}_l^{-1} \mathbf{D}_{l\beta} \tilde{\mathbf{C}}_l^{-1}] \,, \tag{17}$$

where the sum is over bands of width Δl in the power spectra and $f_{\rm sky}$ is the amount of sky covered by the survey. Here we have suppressed the (x_i, x_j) indices in a matrix notation and

$$\mathbf{D}_{l\alpha} = \frac{\partial \mathbf{C}_l}{\partial p_\alpha} \,, \tag{18}$$

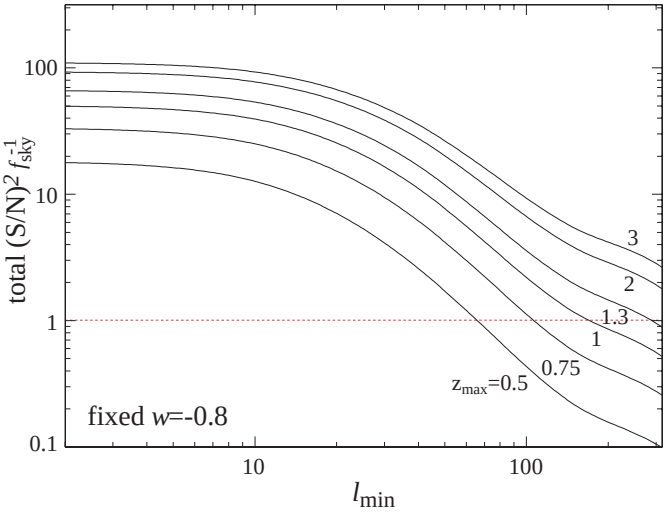

FIG. 7: Total significance of the cross correlation detection for galaxies between $z = 0$ and $z_{\rm max}$ and multipoles $\ell_{\rm min} \le \ell \le 1000$. Half the detection significance is supplied by $z < 1$ galaxies and most of the information comes from $10 \le \ell \le 100$.

where the derivatives are evaluated at a fiducial model through a finite difference approximation. The inverse Fisher matrix approximates the covariance matrix of the parameters $\mathbf{C}^p \approx (\mathbf{F}^{-1})$. We will take as a fiducial model the $w = -0.8$ model of Fig. 3.

For the CMB temperature field Θ, E-polarization field E and galaxy fields in question, we will assume white noise power spectra

$$\begin{aligned} N_l^{g_i g_i} &= \frac{1}{\bar n_A^i}\,, \\ N_l^{\Theta\Theta} &= \left(\frac{\Delta_T}{T_{\rm CMB}}\right)^2 e^{\ell(\ell+1)\theta_{\rm FWHM}/8\ln 2}\,, \\ N_l^{EE} &= \left(\frac{\Delta_P}{T_{\rm CMB}}\right)^2 e^{\ell(\ell+1)\theta_{\rm FWHM}/8\ln 2}\,, \end{aligned} \tag{19}$$

where n_{Ai} is the galaxy number density in bin i. All noise cross power spectra are assumed to vanish. For the CMB, we will take for illustrative purposes noise specifications close to the Planck satellite $\Delta_T = \Delta_P/\sqrt{2} = 40\mu$K-arcmin and $\theta_{\rm FWHM} = 7$ arcmin. The details of this noise choice are not critical as long as the temperature field is sample variance limited out to $\ell \sim$ few $\times 10^2$. For the galaxies, we use the specifications given in the previous section but again the number densities are sufficiently high so as to make the shot noise subdominant for the ℓ range in question.

The total signal to noise in the cross power spectra can be quantified through a simple one parameter family for the spectra

$$\begin{aligned} C_\ell^{\Theta g_i} &= A C_\ell^{\Theta g_i}\Big|_{\rm fid}\,, \\ D_\ell^{\Theta g_i} &= C_\ell^{\Theta g_i}\Big|_{\rm fid} \end{aligned} \tag{20}$$

such that the Fisher matrix in A gives the significance of the detection given a fixed template for the shapes and relative amplitudes of all the cross power spectra

$$\left(\frac{S}{N}\right)^2\Big|_{\rm total} = (\mathbf{C}^p)^{-1}_{AA} = F_{AA}\,. \tag{21}$$

Note that here the noise includes the sample variance of the fields as it represents the signal-to-noise ratio of the correlation detection.

This total significance is shown in Fig. 7 and is approximately 100, or a signal-to-noise ratio of 10 for the full range of $z_{\rm max} < 3$ and $\ell = 2 - 1000$ for a full sky survey $f_{\rm sky} = 1$. Even with multiple power spectra from galaxies across the whole range of the acceleration period, the signal-to-noise remains moderate due to the sample variance of the single CMB temperature field [15].

Note that for the $w = -0.8$ fiducial model roughly half of the information comes from galaxies at $z > 1$ which are accessible only to a very deep survey. (This contribution decreasess somewhat as $w \to -1$ leading to a slightly smaller total signal to noise [15].) On the other hand, doubling the information only increases the signal to noise by $\sqrt{2}$. Furthermore, most of the information comes from intermediate multipoles $10 \lesssim \ell \lesssim 100$ which are accessible to a deep but not necessarily all-sky survey. With increasing redshift, the weight moves to higher ℓ at higher z due to projection effects.

The total signal-to-noise ratio gives a rough quantification of prospects for dark energy clustering constraints. A S/N of 10 implies that the amplitude of the cross power spectrum can be measured to about 10% from the intermediate multipoles. Since the ISW effect is sensitive to the change in the potential, it gains a factor of ~ 3 enhancement in sensitivity to potential variations. Thus roughly the cross correlation can detect a 10% variation in Φ as in the $w = -0.8$ model at $\sim 3\sigma$. This ℓ range implies that this ability applies to a transition scale of $1\% - 10\%$ of the horizon.

This order of magnitude estimate is borne out by a more quantitative treatment. Here we employ the 7 cosmological parameters that determine the fiducial model in Fig. 3 as Fisher parameters. To account for the dark energy clustering we add the sound speed as a parameter. Because the effect of the sound speed is only apparent for variations that span an order of magnitude in c_e, we take this parameter to be

$$p_{c_e} = \frac{\log_{10} c_e}{\Delta \log_{10} c_e}\,, \tag{22}$$

where $\Delta \log_{10} c_e$ is the step away from $c_e = 1$ used to define the parameter derivative in Eq. (18). This normalization factor reflects the fact that the Fisher errors should be interpreted as the significance of the observed difference between the actual models used to define the derivative

$$\left(\frac{S}{N}\right)^2\Big|_{c_e} = (\mathbf{C}^p)^{-1}_{p_{c_e} p_{c_e}}\,. \tag{23}$$

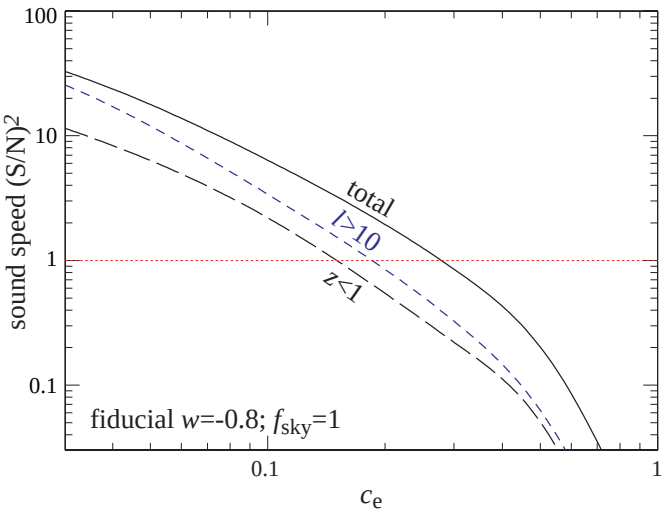

FIG. 8: Significance of the separation between a given c_e model and a quintessence model of $c_e = 1$ given an all sky survey of galaxies and allowing for parameter degeneracies around a $w = -0.8$ model. Note that in comparison with the total detection significance, dark energy clustering model separation requires lower multipoles and utilizes more high-z galaxies as $c_e \to 1$ and the effects are confined to the largest scales.

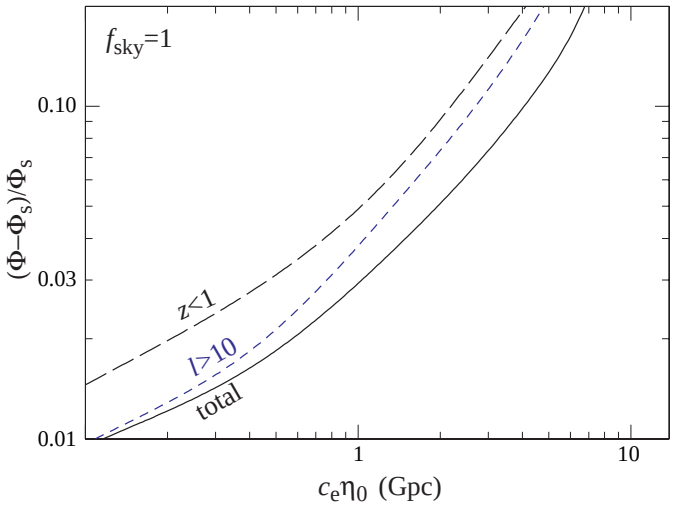

FIG. 9: Conversion of the sound speed constraints into more robust dark energy smoothness constraints. Shown are the projected 1σ errors on the change in the gravitational potential due to dark energy clustering as a function of scale. The galaxy-ISW correlation can ultimately constrain the smoothness of the dark energy at the 1Gpc scale to $\sim 3\%$ in the potential.

accounting for parameter degeneracies.

To these cosmological parameters, we supplement 5 additional "nuisance" parameters per galaxy redshift bin that define the galaxy bias. These parameters, given explicitly in [23], define the occupation of galaxies in dark matter halos. We then have a total of 58 parameters. Though marginalization of these extra parameters can in general degrade constraints due to parameter degeneracies, in this case the information in the auto power spectra of the CMB and galaxies suffices to make the constraints quite comparable to those from employing the cross power spectrum only but with the other parameters fixed. The addition of the galaxy auto correlation power spectrum actually enhances the significance of the separation between $c_e = 1$ and $c_e \ll 1$ models and begins to play a role at $c_e \lesssim 0.1$. Similar to massive neutrinos, for very low sound speeds, the transition occurs on scales where the galaxy power spectra are well measured and the ISW effect is negligible. However there may be subtleties in the $c_e \ll 1$ regime involved with galaxy bias as to whether the galaxies trace the total density perturbation or that of the dark matter.

We show the significance of the separation between models with different sound speeds in Fig. 8 including marginalization over w and other parameters. Recall that for the $w = -0.8$ fiducial model shown here the amplitude of the effect is $\sim 10\%$ in the gravitational potential. The model with $c_e = 0.1$ is distinguished at a $S/N \approx 2.5$ for $f_{\rm sky} = 1$. Note however that the significance drops off rapidly as $c_e \to 1$ as the changes become confined to the low multipoles. Thus one would draw an incorrect inference if one employed $\log_{10} c_e$ directly as a Fisher parameter and let the derivative be approximated by finite difference with $\Delta \log_{10} c_e \to 0$.

Utilization of the ISW-galaxy correlation for dark energy clustering does shift the optimal redshift and multipole range to higher redshifts and lower multipoles compared with a simple detection significance criteria. Because the effects are confined to large physical scales, they can only be observed out to a certain maximum ℓ which increases with redshift due to projection effects (see Fig. 5). The effect of losing the lowest multipoles due to survey boundaries or systematic effects or the highest redshifts due to depth and photometric redshift errors is thus more substantial for distinguishing between clustering models (see Fig. 8).

These results remain robust when varying the fiducial model in w if interpreted as the significance of detecting a given variation in the gravitational potential due to dark energy clustering on scales corresponding to $c_e\eta_0 \approx 14 c_e$ Gpc. We show this rescaling of Fig. 9 to $S/N = 1$ for effective 1σ errors on the change in the gravitational potential due to dark energy clustering out to a given scale. The caveat is that as $w \to -1$ one would predict no change out through the horizon in an adiabatic model. These results are also robust to changes in the halo model for galaxy bias, variations in the galaxy source density, and improvements in photometric redshift accuracy.

V. DISCUSSION

The ISW effect provides a unique probe of the dynamics of the dark energy through its high sensitivity to the smoothness of the dark energy. Although the significance of its detection through cross correlation with galaxy surveys or gravitational lensing statistics will never exceed $\sim 10\sigma$ due to the cosmic variance of the CMB temperature field [15], it is likely to be the best means of probing the clustering dynamics since their effects appear only on the largest scales.

A 10σ detection of the correlation will allow its measurement to $\sim 10\%$ and hence yield the ability to limit $\sim 3\%$ variations in the gravitational potential due to the dark energy clustering if they appear on the Gpc scale. In the adiabatic model, this would allow for a test of the quintessence, or canonical single scalar field, hypothesis if $|1+w| \gtrsim 0.05$. For distinguishing clustering models, as opposed to a simple detection of the correlation, it is important to measure correlation at the largest angles out to $z \sim 2$. That will require a deep nearly all-sky survey such as LSST [25]. Furthermore the galaxy clustering signal on very large angles is itself small and controlling systematics in the galaxy surveys will pose a significant challenge (e.g. [26, 27]).

Finally, beyond the adiabatic model, clustering in the dark energy may have strong effects even if $w \to -1$. For example, in the isocurvature models designed to suppress the quadrupole [21, 28], the change in the gravitational potential is about 6 times that of the adiabatic model. Such models are potentially testable with CMB-galaxy cross correlations in the right redshift range. Likewise explanations for the acceleration that involve modifications to gravity in place of the dark energy may predict a different CMB-galaxy correlation on the largest scales. The uniqueness of this probe of the acceleration of the expansion should motivate future studies despite challenges facing its exploitation.

Acknowledgments: We thank J. Carlstrom, L. Pogosian, C. Gordon, and A. Stebbins for useful discussions. WH was supported by the DOE and the Packard Foundation. RS was partially supported by NSF CAREER award AST99 84924 and NSF ITR ACI-0121671. A portion of this work was carried out at the KICP under NSF PHY-0114422.

[1] R. Caldwell, R. Dave, and P. Steinhardt, Phys. Rev. Lett. **80**, 1582 (1998), astro-ph/9708069.
[2] W. Hu, Astrophys. J. **506**, 485 (1998), astro-ph/9801234.
[3] R. Sachs and A. Wolfe, Astrophys. J. **147**, 73 (1967).
[4] L. Kofman and A. Starobinskii, Sov. Astron. **11**, 271 (1985).
[5] C. Bennett et al., Astrophys. J. Sup. **148**, 1 (2003).
[6] R. Bean and O. Dore, Phys. Rev. D **69**, 083503 (2004), astro-ph/0307100.
[7] R. Crittenden and N. Turok, Phys. Rev. Lett. **76**, 575 (1996).
[8] D. Goldberg and D. Spergel, Phys. Rev. D **59**, 103002 (1999), astro-ph/9811251.
[9] U. Seljak and M. Zaldarriaga, Phys. Rev. D **60**, 043504 (1999), astro-ph/9811123.
[10] W. Hu, Phys. Rev. D **65**, 023003 (2002), astro-ph/0108090.
[11] S. Boughn and R. Crittenden, Nature **427**, 45 (2004).
[12] P. Fosalba and E. Gaztanaga, Mon. Not. R. Astron. Soc. **350**, 37 (2004).
[13] R. Scranton et al., Astrophys. J. in press (2004), astro-ph/0307335.
[14] N. Afshordi, Y.-S. Loh, and M. Strauss, Phys. Rev. D **69**, 083524 (2004).
[15] N. Afshordi, Astrophys. J. in press (2004), astro-ph/0401166.
[16] J. Bardeen, Phys. Rev. D **22**, 1882 (1980).
[17] W. Hu and D. Eisenstein, Phys. Rev. D **52**, 083509 (1999), astro-ph/9809368.
[18] J. Garriga and V. Mukhanov, Phys. Lett. B **458**, 219 (1999), hep-th/9904176.
[19] S. Dedeo, R. Caldwell, and P. Steinhardt, Phys. Rev. D **67**, 103509 (2003).
[20] C. Armendariz-Picon, V. Mukhanov, and P. Steinhardt, Phys. Rev. Lett. **85**, 4438 (2000), astro-ph/0004134.
[21] C. Gordon and W. Hu, Phys. Rev. D submitted (2004), astro-ph/0406496.
[22] J. Weller and A. M. Lewis, Mon. Not. Roy. Astron. Soc. **346**, 987 (2003), astro-ph/0307104.
[23] W. Hu and B. Jain, Phys. Rev. D in press (2003), astro-ph/0312395.
[24] D. Spergel et al., Astrophys. J. Sup. **148**, 175 (2003), astro-ph/0302209.
[25] Dark matter telescope: http://www.dmtelescope.org.
[26] S. J. Maddox, G. Efstathiou, and W. J. Sutherland, Mon. Not. R. Astron. Soc. **246**, 433 (1990).
[27] R. Scranton et al., Astrophys. J. in preparation (2004).
[28] T. Moroi and T. Takahashi, Phys. Rev. Lett. **92**, 091301 (2004), astro-ph/0308208.